Enhanced ^{1}H-X D-HMQC Performance through Improved ^{1}H Homonuclear Decoupling

Frédéric A. Perras[1], Tian Wei Goh,[1,2] Lin-Lin Wang,[1] Wenyu Huang,[1,2] and Marek Pruski[1,2]*

[1]US Department of Energy, Ames Laboratory, Ames, IA, 50011, USA

[2]Department of Chemistry, Iowa State University, Ames, IA, 50011, USA

*Author to whom correspondence should be addressed

Email: mpruski@iastate.edu

Abstract

The sensitivity of solid-state NMR experiments that utilize ^{1}H zero-quantum heteronuclear dipolar recoupling, such as D-HMQC, is compromised by poor homonuclear decoupling. This leads to a rapid decay of recoupled magnetization and an inefficient recoupling of long-range dipolar interactions, especially for nuclides with low gyromagnetic ratios. We investigated the use, in symmetry-based ^{1}H heteronuclear recoupling sequences, of a basic *R* element that was principally designed for efficient homonuclear decoupling. By shortening the time required to suppress the effects of homonuclear dipolar interactions to the duration of a single inversion pulse, spin diffusion was effectively quenched and long-lived recoupled coherence lifetimes could be obtained. We show, both theoretically and experimentally, that these modified sequences can yield considerable sensitivity improvements over the current state-of-the-art method and applied them to the indirect detection of ^{89}Y in a metal-organic framework.

Keywords

Heteronuclear correlation, homonuclear decoupling, solid-state NMR, symmetry-based recoupling

Graphical Abstract

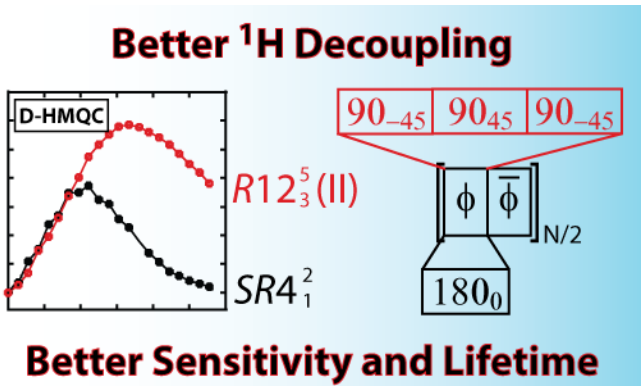

1. Introduction

Solid-state nuclear magnetic resonance (SSNMR) spectroscopy, diffraction techniques, and, in some cases, electron microscopy are the primary techniques available for the interrogation of the atomic-level structures of solid materials. Among these, only SSNMR is able to explore the atomic-level structures of non-crystalline or disordered materials such as glasses,[1] heterogeneous catalysts,[2-4] and battery cathode materials,[5,6] just to name a few. SSNMR has also been used to determine, or refine, the crystalline structures of microcrystalline materials that cannot be solved by powder diffraction techniques; an area called NMR crystallography.[7-9]

SSNMR's main structural handle is the acquisition of 2D homonuclear and heteronuclear correlation (HETCOR) data, which yield information regarding the bonding networks of the material as well as the proximities, and specific distances, between the various sites. While, in principle, the three-dimensional structure of any material can be solved through the acquisition of extensive correlation data,[10-17] experimental challenges, especially poor sensitivity, prevent the practical realization of this approach. Multiple classes of dipolar-based (through-space) HETCOR techniques have thus been developed over the last few decades to both improve the sensitivity and information content of spectra.

The first class of techniques makes use of cross-polarization (CP) for the transfer of magnetization from one nucleus to the other.[18-22] This approach is robust and typically provides the highest sensitivity when considering pairs of spin-1/2 nuclei.[23,24] It has also been modified to enable ^{1}H detection under fast magic-angle-spinning (MAS) in the indirectly-detected HETCOR (idHETCOR) sequence.[25-27] Despite these strengths, CP-HETCOR approaches have a relatively

narrow spectral bandwidth and show significantly reduced sensitivity and reliability when applied to quadrupolar nuclei, due to the requirement that those nuclei be spin-locked.[28-30]

To address the drawbacks of the CP-HETCOR approaches, HETCOR methods utilizing γ-encoded[31] and non-γ-encoded dipolar recoupling have been developed. The techniques making use of γ-encoded recoupling make use of the PRESTO[32-35] (phase-shifted recoupling effects a smooth transfer of order) and D-HUQC[36] (dipolar-heteronuclear universal quantum correlation) pulse sequences, which yield a direct polarization transfer and the indirect detection of heteronuclear n-tuple-quantum coherences (with n = 0, 1 and 2), respectively. While these techniques can provide high sensitivity as well as robustness to spinning instabilities, γ-encoded heteronuclear dipolar recoupling is severely dipolar-truncated,[33] which prevents them from being used to detect long-range correlations. Alternatively, non-γ-encoded heteronuclear dipolar recoupling can be implemented in sequences such as D-RINEPT[37-39,40,31,24] (dipolar-refocused insensitive nuclei enhanced by polarization transfer) for polarization transfer and D-HMQC[41,42] (dipolar-heteronuclear multiple-quantum correlation) for the indirect detection of heteronuclear multiple-quantum coherences. Unlike their γ-encoded counterparts, these techniques do not suffer from dipolar truncation and can thus enable the detection of long-range coherences as well as the measurement of greater distances. The D-HMQC experiment, in particular, has found widespread use for the acquisition of HETCOR spectra involving ^{14}N[41,43-54] and half-integer quadrupolar nuclei.[40,55-57] More recently, its broadbandedness has also been exploited for the detection of correlations to ultra-wideline and isotropic spectra of heavy spin-1/2 nuclei[58,59] as well as satellite transitions of quadrupolar nuclei.[60,61]

Despite the abovementioned advantages, the D-RINEPT and D-HMQC techniques are limited by the lack of radiofrequency (RF) power flexibility of non-γ-encoded heteronuclear

dipolar recoupling sequences. While a near continuum of γ-encoded heteronuclear recoupling sequences (that also decouple homonuclear dipolar interactions) exists with both high- and low-radiofrequency (RF) requirements, non-γ-encoded heteronuclear dipolar recoupling sequences are limited to low RF power ($\nu_{RF} = 2\nu_R$ or $4/3\nu_R$, where ν_R denotes the MAS spinning frequency).[62] While this has been heralded as a boon for fast MAS, such low RF powers pose challenges when those techniques are applied to ^{1}H spins whose strong homonuclear dipolar coupling interactions overpower the weak RF fields. In such cases, the heteronuclear recoupling sequence can be seen to insufficiently decouple ^{1}H spins thus leading to rapid decoherence and a loss in sensitivity.

To address this drawback, we have sought to improve the efficiency of the ^{1}H homonuclear decoupling in these sequences by introducing basic *R* elements that perform homonuclear decoupling into some commonly used *R*-type symmetry-based recoupling sequences. We hypothesize that by shortening the timescale in which the homonuclear dipolar coupling is refocused, we should be able to quench ^{1}H-^{1}H spin diffusion and slow the decoherence of the ^{1}H magnetization to improve sensitivity.

2. Theory

The pulse sequence diagram for the D-HMQC sequence is depicted in Figure 1a. The sequence is essentially identical to the *J*-based HMQC sequence,[63] commonly used in liquid-state NMR, with the exception that zero-quantum heteronuclear dipolar recoupling is applied during the *J* evolutions to reintroduce the heteronuclear dipolar couplings. Under the action of this recoupling the dipolar interaction behaves analogously to *J* coupling and thus the transition from solution-state sequences to their corresponding solid-state, dipolar-based, analogs is fairly straightforward.

Although a number of recoupling sequences have been proposed for D-HMQC, including R^3 and SFAM[64] (simultaneous frequency and amplitude modulation),[65] by far the most popular ones have been those making use of *R*-type symmetry-based recoupling. An RN^{ν}_{n} sequence is composed of N/2 pairs of two pulse elements ($R_{\phi}R_{-\phi}$) that each performs a 180° rotation about the specified phase (where $\phi = \pi\nu/N$) and have durations of nt_R/N, where $t_R = (\nu_R)^{-1}$.[62,66] An *N* number of *R* elements are thus applied for a complete cycle lasting *n* rotor periods (see Figure 1b). The simplest basic *R* element corresponds to a single π pulse, although numerous composite *R* elements have been developed to minimize the influence of RF imperfections, or to improve the selectivity of the recoupling sequence.[62,67]

The selectivity of the RN^{ν}_{n} sequence to the desired interaction can also be enhanced through the application of a supercycle wherein the RN^{ν}_{n} sequence is repeated with an incremented, or inverted, phase.[68,69,70] This equates to nesting the *R*-sequence within a *C*-type symmetry-based recoupling sequence, thus superimposing each sequence's respective selection criteria.

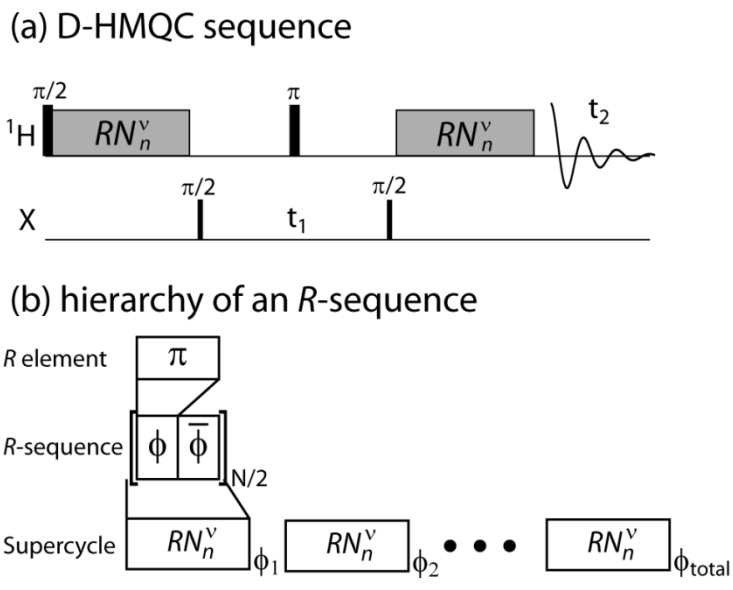

Figure 1. The pulse sequence diagram for the D-HMQC sequence is depicted in (a) while the general hierarchy of an *R*-sequence is shown in (b).

There are thus 3 levels in an RN^{ν}_{n} sequence during which it is possible to suppress undesired interactions: the basic *R* element, the *R*-sequence, and the supercycle. In the case of homonuclear dipolar decoupling, it is most critical to refocus the dipolar interaction on the shortest timescale possible to quench spin diffusion and prevent decoherence. As such, we would expect the best performance from sequences in which the basic *R* element level is tasked with performing the homonuclear decoupling, and the worst in those that achieve homonuclear decoupling through the use of supercycling.

We will consider 2 RN^{ν}_{n} sequences that have been proposed for ^{1}H-X D-HMQC experiments: $R4^{2}_{1}$ and $R12^{5}_{3}$, which both provide non-γ-encoded zero-quantum recoupling of heteronuclear dipolar interactions with the same scaling factor of 0.204.[65,71] However, $R4^{2}_{1}$ also reintroduces homonuclear dipolar interactions with a scaling factor of 0.106. In order to counter this, Brinkmann et al. supercycled the $R4^{2}_{1}$ sequence as follows: $\{R4^{2}_{1}\ R4^{-2}_{1}\}_{0}\ \{R4^{2}_{1}\ R4^{-2}_{1}\}_{120}\ \{R4^{2}_{1}\ R4^{-2}_{1}\}_{240}$, which equates to nesting the $R4^{2}_{1}$, $C2^{1}_{2}$, and $C3^{1}_{6}$ symmetries.[72] Both $C2^{1}_{2}$ and $C3^{1}_{6}$ refocus the homonuclear dipolar terms that are $R4^{2}_{1}$-allowed and thus, through the application of this supercycle, a similar transfer efficiency as $R12^{5}_{3}$ can be obtained with the $R4^{2}_{1}$ sequence. This sequence is commonly known as $SR4^{2}_{1}$ and is currently by far the most utilized heteronuclear zero-quantum recoupling sequence.

Despite the proven efficacy of the aforementioned supercycle, it is disconcerting that homonuclear dipolar interactions are actively recoupled in $SR4^{2}_{1}$ on a timescale lasting 1 rotor period. It then takes a full 2 rotor periods, or 50 μs at $\nu_{R} = 40$ kHz, for the ^{1}H-^{1}H dipolar interactions

to be fully refocused. By comparison, with $R12^5_3$ the homonuclear dipolar interactions are not allowed to evolve and thus, contrary to $SR4^2_1$, by the end of the first rotor period there are no homonuclear dipolar terms that need to be refocused. It thus stands that $R12^5_3$ refocuses homonuclear dipolar terms at a rate that is at least twice that of $SR4^2_1$.[71] Furthermore, if we were able to refocus these interactions at the basic R element level, homonuclear decoupling could be achieved 8 times faster (in just 6.25 μs at ν_R = 40 kHz), in which case the rate of ^{1}H-^{1}H decoupling would become comparable to the strength homonuclear dipolar interactions. Madhu and co-workers have designed such a composite pulse for the acquisition of high-resolution ^{1}H MAS spectra: $R = 90_{-45}90_{45}90_{-45}$.[73,74,75,76] The introduction of this R element into the $R12^5_3$ and $SR4^2_1$ sequences (henceforth referred to as $R12^5_3$(II) and $SR4^2_1$(II)) increases the RF power requirement to $3\nu_R$ and slightly decreases the heteronuclear dipolar recoupling scaling factor to 0.156.

The conventional phases for $R12^5_3$(II), where the phases in the second R element are simply inverted (i.e. $[R_\phi]_0[R_{-\phi}]_0$), correspond to:

$$R12^5_3(\text{II}) = \{90_{30}90_{120}90_{30}90_{330}90_{240}90_{330}\}. \quad (1)$$

The same recoupling sequence can, however, be represented using a different set of phases. In $R12^5_3$ the phase shift (ϕ) corresponds to 75° and thus instead of inverting the phases of all pulses in the second R element, we can obtain an equivalent element by simply subtracting 2ϕ (150°) from all the phases of the first element (i.e. $[R_\phi]_0[R_\phi]_{-2\phi}$). This unconventional cycle was observed through simulation (see supplementary material) to have a superior performance:

$$R12^5_3(\text{II}) = \{90_{30}90_{120}90_{30}90_{240}90_{330}90_{240}\}. \quad (2)$$

This is because $R12^5_3$ compensates thoroughly for RF imperfections, due to its phase shift of π-$\pi/(2n)$ (here, 150°).[71] By incrementing the second *R* element, this useful feature is maintained. By the same token, $SR4^2_1$(II) can be written as:

$$
\begin{aligned}
SR4^2_1(\mathrm{II}) = \{&90_{45}90_{135}90_{45}90_{225}90_{315}90_{225}90_{45}90_{135}90_{45}90_{225}90_{315}90_{225} \\
&90_{225}90_{315}90_{225}90_{45}90_{135}90_{45}90_{225}90_{315}90_{225}90_{45}90_{135}90_{45} \\
&90_{165}90_{255}90_{165}90_{345}90_{75}90_{345}90_{165}90_{255}90_{165}90_{345}90_{75}90_{345} \\
&90_{345}90_{75}90_{345}90_{165}90_{255}90_{165}90_{345}90_{75}90_{345}90_{165}90_{255}90_{165} \\
&90_{285}90_{375}90_{285}90_{105}90_{195}90_{105}90_{285}90_{375}90_{285}90_{105}90_{195}90_{105} \\
&90_{105}90_{195}90_{105}90_{285}90_{375}90_{285}90_{105}90_{195}90_{105}90_{285}90_{375}90_{285}\}. \qquad (3)
\end{aligned}
$$

We first sought to verify the usefulness of these modified recoupling sequences using spin dynamics simulations. We opted to use the same model system as was used by Hu and coworkers when comparing various recoupling sequences for applications with D-HMQC.[65] The model consists of one ^{15}N spin and two ^{1}H spins with a weak ^{15}N-^{1}H dipolar coupling of 1 kHz and a strong ^{1}H-^{1}H dipolar coupling of 25 kHz. Due to the different specifications of our probe, we performed the simulations at a lower MAS rate of 40 kHz.

As can be seen from Figure 2, as the RF power is altered each sequence produces discrete maxima at the expected matching conditions. As previously observed,[65] the $SR4^2_1$ sequence also features efficient recoupling when $\nu_{RF} = 3\nu_R$. Surprisingly, all four sequences yield nearly identical recoupling efficiencies when the RF power is properly set, the principal difference being in their tolerances to RF offsets. Given that some modern probes have large RF inhomogeneities,[77,78] the importance of recoupling sequences that are tolerant to RF maladjustments cannot be overstated.[79] In case where the dominant interaction is the homonuclear dipolar interaction between the two ^{1}H

spins, it is unsurprising that the more tolerant sequence is one that performs homonuclear decoupling on the shortest timescale ($R12^5_3$). The use of a composite pulse *R* element to further improve the homonuclear decoupling efficiency is seen to have the effect of broadening the matching condition for both the $R12^5_3$ and $SR4^2_1$ sequences. These sequences are thus expected to provide a better sensitivity in D-HMQC experiments than their parent counterparts.

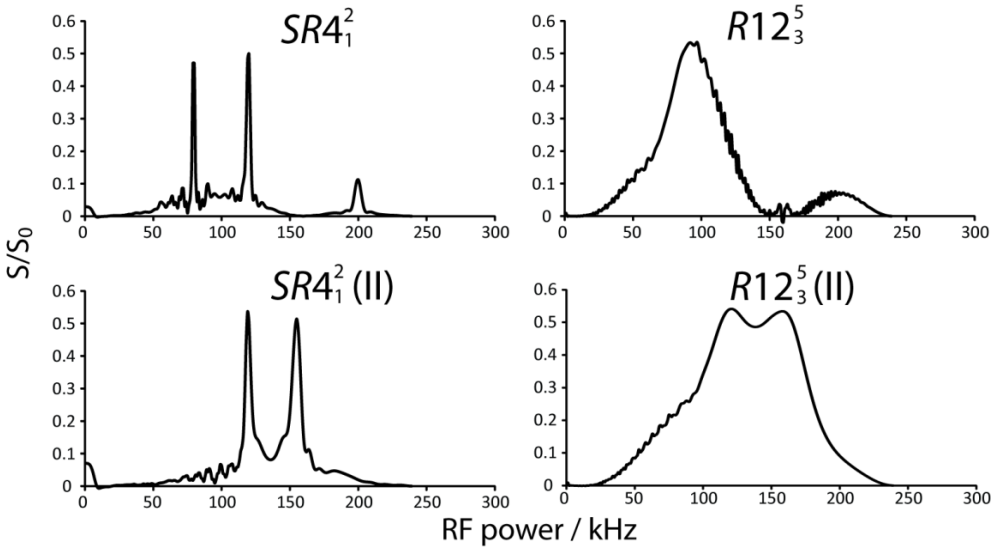

Figure 2. The calculated optimum ^{1}H-^{15}N D-HMQC efficiency, S/S_0, defined as the ratio between the recoupled signal intensity and that obtained using a 90° pulse, is plotted as a function of the recoupling rf power. Data are shown for both the $SR4^2_1$ (left) and $R12^5_3$ (right) recoupling sequences using either a 180_0 (top) or a $90_{-45}90_{45}90_{-45}$ (bottom) basic *R* element.

More importantly, however, the composite pulse-based recoupling sequences are predicted to have far longer coherence lifetimes, something that should facilitate the detection of long-range correlations, or the measurement of distances. Examples of recoupling curves are shown in Figure 3 for an arbitrary 4-spin system. As can be seen from those curves, even though the maximum intensity is practically identical, in agreement with Figure 2 and previously published results, the

two curves diverge at long recoupling times, with the sequences using composite pulse *R* elements providing longer-lived coherences.

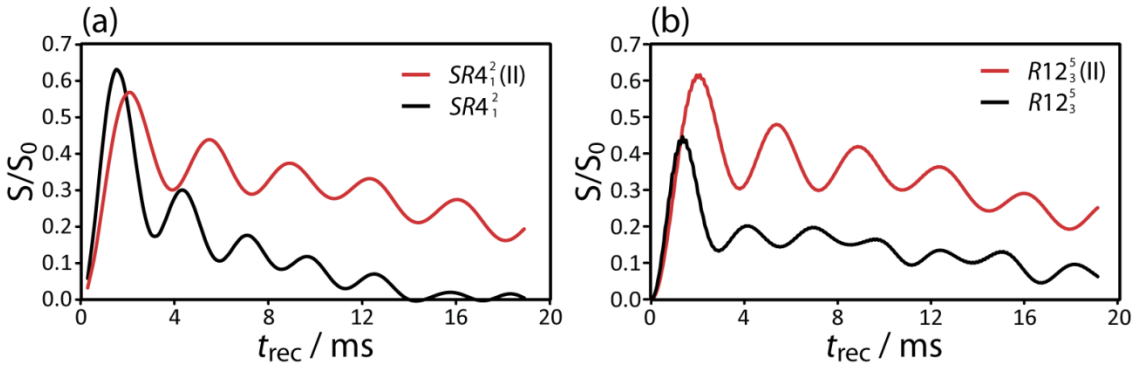

Figure 3. Predicted D-HMQC recoupling curves for an arbitrary 4-spin system consisting of 3 ^{1}H spins and a lone X spin-1/2 nuclide. The X spin is coupled to the first ^{1}H with a dipolar coupling constant of 1.5 kHz and that ^{1}H spin is coupled to the other three ^{1}H spins with dipolar coupling constants of 15, 5, and 7 kHz. Curves calculated using $SR4^{1}_{2}$ (a) and $R12^{5}_{3}$ (b) are shown with those using 180_{0} and $90_{-45}90_{45}90_{-45}$ basic *R* elements in black and red, respectively.

3. Results and Discussion

We opted to test the performance of the new composite pulse zero-quantum heteronuclear recoupling sequences using uniformly ^{13}C- and ^{15}N-enriched histidine hydrochloride monohydrate. The ^{1}H-^{13}C and ^{1}H-^{15}N recoupling curves for the 5 ^{1}H resonances that are resolved at 36 kHz MAS are shown in Figure 4 using $R4^{2}_{1}$ as well as both the 180_{0} and $90_{-45}90_{45}90_{-45}$ variants of $R12^{5}_{3}$ and $SR4^{2}_{1}$. As can be seen, when the recoupled spins are directly bound to one another the maximum recoupling efficiency is independent of the recoupling sequence used, except in the case of $R4^{2}_{1}$ which yield weaker signals; nonetheless, the composite pulse sequences yield far longer-lived coherences. Also, the $R12^{5}_{3}$ sequences generally showed better performance

than the $SR4^2_1$ ones. For the cases where the recoupled spins are not directly bound (Figures 4aiv, 4av) or when the dipolar couplings are partly motionally averaged (Figure 4bi) we can see that $R12^5_3$(II) provides the best transfer efficiency. For instance, $R12^5_3$(II) provides a 50% higher intensity than $SR4^2_1$ in the case of ^{13}C and a 35% higher intensity in the case of ^{15}N.

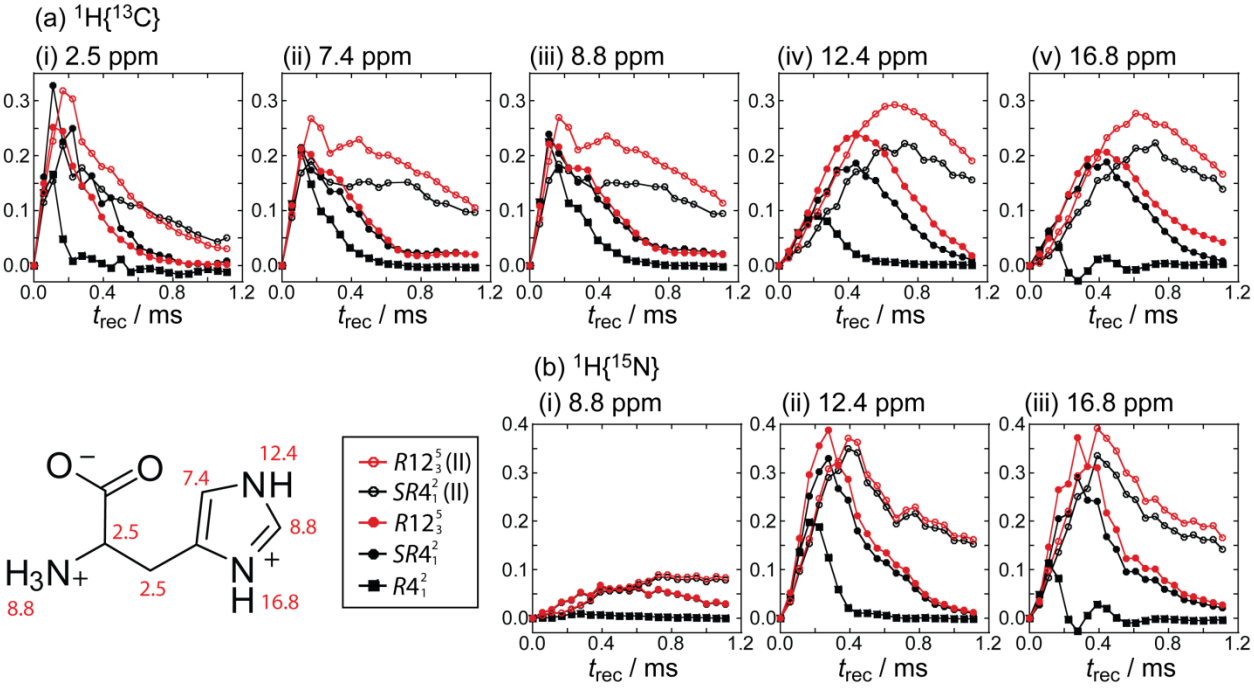

Figure 4. Experimental ^1H-^{13}C (a) and ^1H-^{15}N (b) D-HMQC recoupling curves for a sample of $^{13}C/^{15}N$-enriched histidine HCl monohydrate spinning at 36 kHz. The recoupling curves for the different resolved ^1H resonances, assigned in the structure (bottom left), were acquired by $SR4^2_1$ (black) and $R12^5_3$ (red) using either a 180_0 (filled circles) or $90_{-45}90_{45}90_{-45}$ (empty circles) basic *R* element for the recoupling. Curves for non-supercycled $R4^2_1$ (black squares) are also shown.

Clearly, the significance of proper ^1H-^1H homonuclear decoupling while performing heteronuclear recoupling is best exemplified when recoupling long-range interactions, or when trying to excite coherences involving low-γ nuclides. As such, we have sought to indirectly detect,

through ^{1}H spins, the ^{89}Y SSNMR signal from the yttrium sites in the Y-MOF-76 metal-organic framework (MOF)[80-82] using D-HMQC. Although the sensitivity of D-HMQC may not yet match that of the more conventional CP-based HETCOR approach, it has considerable advantages due to its simplicity of implementation and broad excitation bandwidth. This is particularly important in a case such as this where the chemical shift is unknown.

The ^{1}H-^{89}Y D-HMQC recoupling curves for Y-MOF-76 are depicted in Figure 5a, which shows that $R12^{5}_{3}$(II), despite its slower build-up, manages to deliver 2.5 times greater sensitivity than that obtained using $SR4^{2}_{1}$. This translates into a higher signal-to-noise ratio, and a clearer, 2D ^{1}H-^{89}Y correlation spectrum (Figure 5b and c).

From the 2D ^{1}H-^{89}Y D-HMQC spectrum shown in Figure 5c, we can see that the two crystallographically inequivalent aromatic ^{1}H sites (H1 and H3) are resolved under 36 kHz MAS and that both are correlated to the ^{89}Y signal at 12 ppm. The relative intensity of the two cross-peaks is also reversed from that obtained in a one-dimensional ^{1}H MAS SSNMR spectrum, suggesting that the less abundant site is also the one that is situated closer to the Y cornerstone. Upon inspecting the crystal structure we can see that this is indeed the case with H1, with a relative occupancy of 1, being situated 3.5 Å away from the Y site while H3, with a relative occupancy of 2, is situated 4.3 Å from Y (see Figure 5d). This assignment could be unambiguously confirmed experimentally using a ^{1}H-^{13}C idHETCOR experiment (Figure 5e). In this spectrum, ^{13}C heteronuclear decoupling was not applied and thus the ^{13}C sites bound to H1 and H3 could be identified by their doublet structure in the 2D spectrum (Figure 5f). The remaining ^{13}C sites can be assigned based on their proximities to those sites. The assignments are labeled in Figure 5e and tabulated in Table 1.

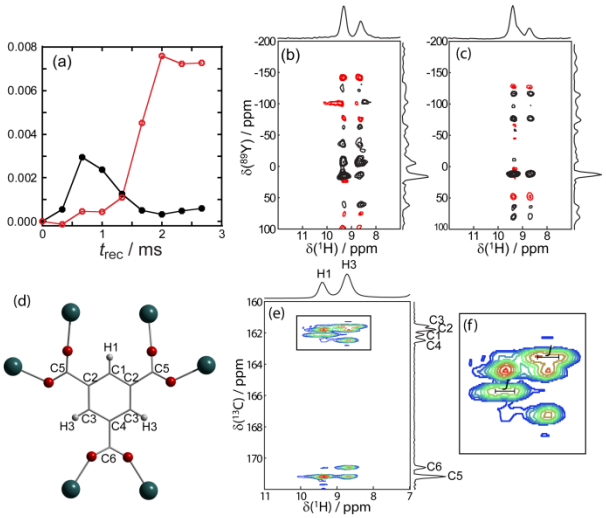

Figure 5. Results from SSNMR experiments on Y-MOF-76. The transfer efficiency, as a function of recoupling time, of a ^{1}H-^{89}Y D-HMQC experiment is shown in (a) when using SR4$^{2}_{1}$ (black) and R12$^{5}_{3}$(II) (red) for the recoupling. The corresponding 2D ^{1}H-^{89}Y correlation spectra are shown in (b) and (c) for SR4$^{2}_{1}$ and R12$^{5}_{3}$(II), respectively. Part of the MOF structure around the benzenetricarboxyl ligand is shown in (d) with hydrogen shown in white, oxygen in red, and yttrium in green. The ^{1}H-^{13}C idHETCOR spectrum used to confirm the assignments of the resonances is shown in (e), with an inset expanded in (f).

Table 1. Experimental and calculated chemical shifts for the various sites in Y- MOF-76.

site	$\delta_{iso,expt.}$ / ppm	$\delta_{iso,calc.}$ / ppm
H1	9.43 ± 0.05	9.42
H2	5.05 ± 0.05	3.12
H3	8.75 ± 0.05	8.87
C1	162.1 ± 0.2	145.8
C2	161.7 ± 0.2	143.6
C3	161.6 ± 0.2	141.3
C4	162.5 ± 0.2	148.2
C5	171.2 ± 0.2	180.7
C6	170.6 ± 0.2	181.1
Y1	12 ± 2	-2.5

We have further confirmed these assignments with the use of the gauge-including projector-augmented-wave (GIPAW) density functional theory (DFT) method.[83-85] The calculated chemical shifts, referenced *in silico* to TMS and aqueous Y^{3+} using molecular TMS and crystalline Y_2O_3,[86] are tabulated in Table 1. Remarkable quantitative agreement was obtained when comparing the ^{1}H chemical shifts of H1 and H3 to the experiment while that of H2, belonging to a coordinated water molecule, was 2 ppm off. This latter disagreement was likely due to the dynamics of water molecules in the pore which would also explain the lack of correlation between the water protons and yttrium in the D-HMQC spectra. A good agreement with the ^{89}Y chemical shift was also obtained, with the two numbers differing by only 14 ppm. Note that the ^{89}Y chemical shift scale spans over 1000 ppm.[87] The ^{13}C chemical shifts were, however, not well reproduced by DFT. The fact that the difference between the aromatic and carboxylate shifts was not reproduced by the calculations suggests that there may be a significant heavy-atom/light-atom effect from the Y sites on the ^{13}C chemical shifts.[88] Relativistic effects on magnetic shielding calculations have yet to be included in the Vienna Atomic Simulation Package (VASP).

4. Conclusions

We investigated the utility of homonuclear dipolar coupling-compensated basic *R* elements for use in ^{1}H non-γ-encoded zero-quantum heteronuclear dipolar recoupling. The composite pulses were shown to improve the D-HMQC coherence lifetimes of both the $SR4^{2}_{1}$ and $R12^{5}_{3}$ recoupling sequences, with the latter having the better performance. Sensitivity improvements of up to 50% were obtained when using $R12^{5}_{3}$(II) to acquire ^{13}C and ^{15}N D-HMQC spectra at 36 kHz MAS for histidine HCl monohydrate, over $SR4^{2}_{1}$. We lastly applied the new $R12^{5}_{3}$(II) sequence to acquire a ^{1}H-^{89}Y D-HMQC spectrum for Y-MOF-76. In this case, due to the low gyromagnetic ratio of ^{89}Y, $R12^{5}_{3}$(II) was able to improve the sensitivity by a factor of 2.5 over $SR4^{2}_{1}$. We expect

these new sequences to open up new opportunities for the indirect detection of low-frequency isotopes in materials. The difference between the composite pulse sequences and the more conventional $SR4^2_1$ sequence is expected to be lessened at ultra-fast MAS rates due to the improved decoupling afforded by the sample spinning itself.

5. Experimental

Y-MOF-76 was prepared according to previously reported procedures[80,81,82] with slight modifications. In a 20 mL Pyrex vial, $Y(NO_3)_3{\cdot}6H_2O$ (383 mg, 1.0 mmol) and benzenetricarboxylic acid (105 mg, 0.5 mmol) were dissolved in 8 mL of N,N-dimethylformamide (DMF) and 8 mL of water. The vial was sealed and incubated in a 105 °C oven. After 24 h, the white crystalline precipitate was isolated by centrifugation at 7000 rpm for 10 minutes. This precipitate was then washed with copious amounts of water and acetone to remove the unreacted starting materials. The washed sample was dried in an oven at 100 °C.

All SSNMR experiments were performed on a 600 MHz Varian NMR system equipped with a 1.6-mm fast-MAS probe. Samples were packed into 1.6-mm zirconia rotors and spun at 36 kHz. The ^{1}H RF power for all hard pulses was set to 108 kHz while those for ^{13}C and ^{15}N were set to 100 kHz and those for ^{89}Y to 83.3 kHz. The RF power for the standard recoupling sequences was set to 72 kHz but increased to 108 kHz for the composite sequences. The ^{1}H-^{89}Y D-HMQC spectra were acquired in 64 t_1 increments of 55.56 μs with each increment consisting of 2048 scans using the aforementioned parameters and total recoupling times of 0.67 and 2 ms for $SR4^2_1$ and $R12^5_3$(II), respectively. The States-TPPI method was used for phase-sensitive detection. The ^{1}H-^{13}C idHETCOR spectrum was acquired using a previously published sequence[27] with an initial contact time of 2.5 ms and a second contact time of 600 μs. HORROR was applied for 8.2 ms

prior to the second contact to destroy any uncorrelated ^{1}H magnetization. A total of 512 t_1 increments of 27.78μs, each consisting of 80 scans, were acquired and the States-TPPI method was used for phase-sensitive detection. The recycle delays were set of 4 and 0.4 s for histidine HCl monohydrate and Y-MOF-76, respectively.

Spin dynamics simulations were performed using SIMPSON (ver. 4.1.1).[89,90] The spinning frequency was set to 40 kHz and the dipolar interactions were set to those given in the main text. Powder averaging was performed using 100 orientations calculated by REPULSION,[91] as well 4 γ-angles. All recoupling pulses were explicitly calculated while ideal pulses were assumed for the refocusing ^{1}H pulse as well as the two X pulses.

DFT[92,93] calculations of Y-MOF-76 were performed using PBE[94] in a plane-wave basis set and the projector augmented wave method,[95] as implemented in the VASP.[96,97] Magnetic shieldings were calculated using the GIPAW method.[98,83] The Y-MOF-76 tetragonal unit cell has a total of 88 atoms including 4 water molecules, each coordinated to a Y site. A kinetic energy cutoff of 500 eV for the plane-wave basis set and a (3×3×2) Monkhorst-Pack[99] *k*-point mesh with a Gaussian smearing of 0.05 eV were used. All the atoms, as well as the volume of the unit cell, were relaxed until the absolute values of forces were below 0.02 eV/Å. The relaxed unit cell dimensions of a=10.39 and c=14.59 Å were within 1% of the experimental values of 10.29 and 14.50 Å, respectively. In order to get the reference of the chemical shifts for ^{1}H, ^{13}C, and ^{89}Y, a free TMS molecule and the Y_2O_3 in the body-centered cubic structure were also calculated.

6. Acknowledgements

This work was supported by the U.S. Department of Energy (DOE), Office of Science, Basic Energy Sciences, Materials Science and Engineering Division. The Ames Laboratory is operated for the U.S. DOE by Iowa State University under Contract No. DE-AC02-07CH11358.

7. References

[1] M. Edén, NMR studies of oxide-based glasses, 108 (2012) 177-221.

[2] T. Kobayashi, F. A. Perras, I. I. Slowing, A. D. Sadow, M. Pruski, Dynamic nuclear polarization solid-state NMR in heterogeneous catalysis research, ACS Catal. 5 (2015) 7055-7062.

[3] C. Copéret, W.-C. Liao, C. P. Gordon, T.-C. Ong, Active sites in supported single-site catalysts: an NMR perspective, J. Am. Chem. Soc. 139 (2017) 10588-10596.

[4] D. Grekov, T. Vancompernolle, M. Taoufik, L. Delevoye, R. M. Gauvin, Solid-state NMR of quadrupolar nuclei for investigations into supported organometallic catalysts: Scope and frontiers, Chem. Soc. Rev. 47 (2018) 2572-2590.

[5] C. P. Grey, N. Dupré, NMR studies of cathode materials for lithium-ion rechargeable batteries, Chem. Rev. 104 (2004) 4493-4512.

[6] F. Blanc, M. Leskes, C. P. Grey, *In situ* solid-state NMR spectroscopy of electrochemical cells: Batteries, supercapacitors, and fuel cells, Acc. Chem. Res. 46 (2013) 1952-1963.

[7] C. Martineau, J. Senker, F. Taulelle, NMR crystallography, Annu. Rep. NMR Spectrosc. 82 (2014) 1-57.

[8] D. L. Bryce, NMR crystallography: Structure and properties of materials from solid-state nuclear magnetic resonance observables, IUCRJ, 4 (2017) 350-359.

[9] C. Martineau-Corcos, NMR Crystallography: A tool for the characterization of microporous hybrid solids Curr. Opin. Colloid Interface Sci. 33 (2018) 35-43.

[10] D. H. Brouwer, R. J. Darton, R. E. Morris, M. H. Levitt, A solid-state NMR method for solution of zeolite crystal structures, J. Am. Chem. Soc. 127 (2005) 10365-10370.

[11] D. H. Brouwer, Structure solution of network materials by solid-state NMR without knowledge of the crystallographic space group, Solid State Nucl. Magn. Reson. 51-52 (2013) 37-45.

[12] D. H. Brouwer, K. P. Langendoen, A graph theory approach to structure solution of network materials from two-dimensional solid-state NMR data, CrystEngComm, 15 (2013) 8748-8762.

[13] B. Bouchevreau, C. Martineau, C. Mellot-Draznieks, A. Tuel, M. R. Suchomel, J. Trébosc, O. Lafon, J.-P. Amoureux, and F. Taulelle, High-resolution structural characterization of two layered aluminophosphates by synchrotron powder diffraction and NMR crystallographies, Chem. Mater, 25 (2013) 2227-2242.

[14] B. Bouchevreau, C. Martineau, C. Mellot-Draznieks, A. Tuel, M. R. Suchomel, J. Trébosc, O. Lafon, J.-P. Amoureux, F. Taulelle, An NMR-driven crystallography strategy to overcome the computability limit of powder structure determination: A layered aluminophosphate case, Chem. Eur. J. 19 (2013) 5009-5013.

[15] F. Taulelle, B. Bouchevreau, C. Martineau, NMR crystallography driven structure determination: nanoporous materials, CrystEngComm, 15 (2013) 8613-8622.

[16] D. H. Brouwer, J. Van Huizen, NMR crystallography of zeolites: How far can we go without diffraction data? Magn. Reson. Chem. (2018) in press.

[17] K. Märker, M. Pingret, J.-M. Mouesca, D. Gasparutto, S. Hediger, G. De Paëpe, A new tool for NMR crystallography: Complete $^{13}C/^{15}N$ assignment of organic molecules at natural isotopic abundance using DNP-enhanced solid-state NMR, J. Am. Chem. Soc. 137 (2015) 13796-13799.

[18] E. R. H. van Eck, W. S. Veeman, Solid-state 2D-heteronuclear ^{27}Al-^{31}P correlation NMR spectroscopy of aluminophosphate VPI-5, J. Am. Chem. Soc. 115(1993) 1168-1169.

[19] T. Fujiwara, K. Sugase, M. Kainosho, A. Ono, A. Ono, H. Akutsu, ^{13}C-^{13}C and ^{13}C-^{15}N dipolar correlation NMR of uniformly labeled organic solids for the complete assignment of their ^{13}C and ^{15}N signals: An application to adenosine, J. Am. Chem. Soc. 117 (1995) 11351-11352.

[20] K. V. Ramanathan, S. J. Opella, High-resolution ^{13}C-^{14}N and ^{13}C-^{15}N heteronuclear correlation spectroscopy, J. Magn. Reson. 86 (1990) 227-235.

[21] S. H. Wang, S. M. De Paul, L. M. Bull, High-resolution heteronuclear correlation between quadrupolar and spin-1/2 nuclei using multiple-quantum magic-angle-spinning, J. Magn. Reson. 125 (1997) 364-368.

[22] J. Trebosc, J. W. Wiench, S. Huh, V. S.-Y. Lin, M. Pruski, Studies of organically functionalized mesoporous silicas using heteronuclear solid-state correlation NMR spectroscopy under fast magic angle spinning, J. Am. Chem. Soc. 127 (2005) 7587-7593.

[23] M. Shen, S. Wegner, J. Trébosc, B. Hu, O. Lafon, J.P. Amoureux, Minimizing the t_1-noise when using an indirect ^{1}H high-resolution detection of unlabelled samples, Solid State Nucl. Magn. Reson. 87 (2017) 111-116.

[24] A. Venkatesh, M. J. Ryan, A. Biswas, K. C. Boteju, A. D. Sadow, A. J. Rossini, Enhancing the sensitivity of solid-state NMR experiments with very low gyromagnetic ratio nuclei with fast magic angle spinning and proton detection, J. Phys. Chem. A 122 (2018) 5635-5643.

[25] Y. Ishii, R. Tycko, Sensitivity enhancement in solid state ^{15}N NMR by indirect detection with high-speed magic angle spinning, J. Magn. Reson. 142 (2000) 199-204.

[26] Y. Ishii, J. P. Yesinowski, R. Tycko, Sensitivity enhancement in solid-state ^{13}C NMR of synthetic polymers and biopolymers by ^{1}H NMR detection with high-speed magic angle spinning, J. Am. Chem. Soc. 123 (2001) 2921-2922.

[27] J. W. Wiench, C. E. Bronnimann, V. S.-Y. Lin, M. Pruski, Chemical shift correlation NMR spectroscopy with indirect detection in fast rotating solids: studies of organically functionalized mesoporous silicas, J. Am. Chem. Soc. 129 (2007) 12076-12077.

[28] A. J. Vega, MAS NMR spin locking of half-integer quadrupolar nuclei, J. Magn. Reson. 96 (1992) 50-68.

[29] A. J. Vega, CP/MAS of quadrupolar S = 3/2 nuclei, Solid State Nucl. Magn. Reson. 1 (1992) 17-32.

[30] J.-P. Amoureux, M. Pruski, Theoretical and experimental assessment of single- and multiple-quantum cross-polarization in solid state NMR, Mol. Phys. 100 (2002) 1595-1613.

[31] C. Martineau, B. Bouchevreau, F. Taulelle, J. Trébosc, O. Lafon, J. P. Amoureux, High-resolution through-space correlations between spin-1/2 and half-integer quadrupolar nuclei using the MQ-*D*-R-INEPT NMR experiment, Phys. Chem. Chem. Phys. 14 (2012) 7112-7119.

[32] X. Zhao, W. Hoffbauer, J. S. auf der Günne, M. H. Levitt, Heteronuclear polarization transfer by symmetry-based recoupling sequences in solid-state NMR, Solid State Nucl. Magn. Reson. 26 (2004) 57-64.

[33] M. Sardo, R. Siegel, S. M. Santos, J. Rocha, J. R. B. Gomes, L. Mafra, Combining multinuclear high-resolution solid-state MAS NMR and computational methods for resonance assignment of glutathione tripeptide, J. Phys. Chem. A, 116 (2012) 6711-6719.

[34] F. A. Perras, T. Kobayashi, M. Pruski, PRESTO polarization transfer to quadrupolar nuclei: implications for dynamic nuclear polarization, Phys. Chem. Chem. Phys. 17 (2015) 22616-22622.

[35] F. A. Perras, Z. Wang, P. Naik, I. I. Slowing, M. Pruski, Natural abundance ^{17}O DNP NMR provides precise O-H distances and insights into the Brønsted acidity of heterogeneous catalysts, Angew. Chem. Int Ed. 56 (2017) 9165-9169.

[36] H. Nagashima, A. S. L. Thankamony, J. Trébosc, F. Pourpoint, O. Lafon, J. P. Amoureux, γ-Independent through-space hetero-nuclear correlation between spin-1/2 and quadrupolar nuclei in solids, Solid State Nucl. Magn. Reson. 84 (2017) 216-226.

[37] A. W. Hing, S. Vega, J. Schaefer, Transferred-echo double-resonance NMR, J. Magn. Reson. 96 (1992) 205-209.

[38] C. A. Fyfe, K. T. Mueller, H. Grondey, K. C. Wong-Moon, Dipolar dephasing between quadrupolar and spin-1/2 nuclei. REDOR and TEDOR NMR experiments on VPI-5, Chem. Phys. Lett. 199 (1992) 198-204.

[39] J. Trebosc, B. Hu, J.P. Amoureux, Z. Gan, Through-space R^3-HETCOR experiments between spin-1/2 and half-integer quadrupolar nuclei in solid-state NMR, J. Magn. Reson. 186 (2007) 220-227.

[40] A. Venkatesh, M. P. Hanrahan, A. J. Rossini, Proton detection of MAS solid-state NMR spectra of half-integer quadrupolar nuclei, Solid State Nucl. Magn. Reson. 84 (2017) 171-181

[41] Z. Gan, $^{13}C/^{14}N$ heteronuclear multiple-quantum correlation with rotary resonance and REDOR dipolar recoupling, J. Magn. Reson. 184 (2007) 39-43.

[42] G. Tricot, J. Trébosc, F. Pourpoint, R. Gauvin, L. Delevoye, The D-HMQC MAS-NMR technique: An efficient tool for the editing of through-space correlation spectra between quadrupolar and spin-1/2 (^{13}P, ^{29}Si, ^{1}H, ^{13}C) nuclei. Annu. Rep. NMR Spectrosc. 81 (2014) 145-184.

[43] S. Cavadini, S. Antonijevic, A. Lupulescu, G. Bodenhausen, Indirect detection of nitrogen-14 in solid-state NMR spectroscopy, ChemPhysChem, 8 (2007) 1363-1374.

[44] S. Antonijevic, N. Halpern-Manners, Probing amide bond nitrogens in solids using ^{14}N NMR spectroscopy, Solid State Nucl. Magn. Reson. 33 (2008) 82-87.

[45] J.-P. Amoureux, Q. Wang, B. Hu, O. Lafon, J. Trébosc, F. Deng, Rapid analysis of isotopically unmodified amino acids by high-resolution ^{14}N-edited ^{1}H-^{13}C correlation NMR spectroscopy, Chem. Commun. (2008) 6525-6527.

[46] S. Cavadini, Indirect detection of nitrogen-14 in solid-state NMR spectroscopy, Prog. Nucl. Magn. Reson. Spectrosc. 56 (2010) 46-77.

[47] Y. Nishiyama, Y. Endo, T. Nemoto, H. Utsumi, K. Yamauchi, K. Hioka, T. Asakura, Very fast magic angle spinning ^{1}H-^{14}N 2D solid-state NMR: Sub-micro-liter sample data collection in a few minutes, J. Magn. Reson. 208 (2011) 44-48.

[48] J. A. Jarvis, I. M. Haies, P. T. F. Williamson, M. Carravetta, An efficient NMR method for the characterization of ^{14}N sites through indirect ^{13}C detection, Phys. Chem. Chem. Phys. 15 (2013) 7613-7620.

[49] X. Lu, J. Trébosc, O. Lafon, D. Carnevale, S. Ulzega, G. Bodenhausen, J.-P. Amoureux, Broadband excitation in solid-state NMR using interleaved DANTE pulse trains with *N* pulses per rotor period, J. Magn. Reson. 236 (2013) 105-116.

[50] M. Shen, J. Trébosc, O. Lafon, Z. Gan, F. Pourpoint, B. Hu, Q. Chen, J.-P. Amoureux, Solid State Nucl. Magn. Reson. 72 (2015) 104-117.

[51] E. Dib, T. Mineva, B. Alonso, Recent Advances in ^{14}N solid-state NMR Annu. Rep. NMR Spectrosc. 87 (2016) 175-235.

[52] M. Shen, Q. Chen, J.-P. Amoureux, B. Hu, Broad-band excitation in indirectly detected ^{14}N overtone spectroscopy with composite pulses, Solid State Nucl. Magn. Reson. 78 (2016) 5-8.

[53] A. J. Pell, K. J. Sanders, S. Wegner, G. Pintacuda, C. P. Grey, Low-power broadband solid-state MAS NMR of ^{14}N, J. Chem. Phys. 146 (2017) 194202.

[54] J. A. Jarvis, I. Haies, M. Lelli, A. J. Rossini, I. Kuprov, M. Carravetta, P. T. F. Williamson, Measurement of ^{14}N quadrupole couplings in biomolecular solids using indirect-detection ^{14}N solid-state NMR with DNP, Chem. Commun. 53 (2017) 12116-12119.

[55] J.P. Amoureux, J. Trébosc, L. Delevoye, O. Lafon, B. Hu, Q. Wang, Solid State Nucl. Magn. Reson. 35 (2009) 12-18.

[56] O. Lafon, Q. Wang, B. Hu, F. Vasconcelos, J. Trébosc, S. Cristol, F. Deng, J.-P. Amoureux, Indirect detection via spin-1/2 nuclei in solid-state NMR spectroscopy: Application to the observation of proximities between protons and quadrupolar nuclei, J. Phys. Chem. A, 113 (2009) 12864-12878.

[57] X. Lu, O. Lafon, J. Trébosc, G. Tricot, L. Delevoye, F. Méar, L. Montagne, J.P. Amoureux, Observation of proximities between spin-1/2 and quadrupolar nuclei: Which heteronuclear dipolar recoupling method is preferable? J. Chem. Phys. 137 (2012) 144201.

[58] A. J. Rossini, M. P. Hanrahan, M. Thuo, Rapid acquisition of wideline MAS solid-state NMR spectra with fast MAS, proton detection, and dipolar HMQC pulse sequences, Phys. Chem. Chem. Phys. 18 (2016) 25284-25295.

[59] F. A. Perras, A. Venkatesh, M. P. Hanrahan, T. W. Goh, W. Huang, A. J. Rossini, M. Pruski, Indirect detection of infinite-speed MAS solid-state NMR spectra, J. Magn. Reson. 276 (2017) 95-102.

[60] J. Trébosc, O. Lafon, B. Hu, J.-P. Amoureux, Indirect high-resolution detection for quadrupolar spin-3/2 nuclei in dipolar HMQC solid-state NMR experiments, Chem. Phys. Lett. 496 (2010) 201-207.

[61] N. T. Duong, Y. Nishiyama, Satellite and central transitions selective $^{1}H/\{^{27}Al\}$ D-HMQC experiments at very fast MAS for quadrupolar couplings determination, Solid State Nucl. Magn. Reson. 84 (2017) 83-88.

[62] M. H. Levitt, Symmetry-based pulse sequences in magic-angle spinning solid-state NMR, Encyclopedia of Magnetic Resonance, 9 (2002) 165-196.

[63] A. Bax, R. H. Griffey, B. L. Hawkins, Correlation of proton and nitrogen-15 chemical shifts by multiple quantum NMR, J. Magn. Reson. 55 (1983) 301-315.

[64] R. Fu, S. A. Smith, G. Bodenhausen, Recoupling of heteronuclear dipolar interactions in solid state magic-angle spinning NMR by simultaneous frequency and amplitude modulation, Chem. Phys. Lett. 272 (1997) 361-369.

[65] B. Hu, J. Trébosc, J.P. Amoureux, Comparison of several hetero-nuclear dipolar recoupling NMR methods to be used in MAS HMQC/HSQC, J. Magn. Reson. 192 (2008) 112-122.

[66] M. Carravetta, M. Edén, X. Zhao, A. Brinkmann, M. H. Levitt, Symmetry principles for the design of radiofrequency pulse sequences in the nuclear magnetic resonance of rotating solids, Chem. Phys. Lett. 321 (2000) 205-215.

[67] M. K. Pandey, M. Malon, A. Ramamoorthy, Y. Nishiyama, Composite-180° pulse-based symmetry sequences to recouple proton chemical shift anisotropy tensors under ultrafast MAS solid-state NMR spectroscopy, J. Magn. Reson. 250 (2015) 45-54.

[68] A. Brinkmann, J. S. auf der Günne, M. H. Levitt, Homonuclear zero-quantum recoupling in fast magic-angle spinning nuclear magnetic resonance, J. Magn. Reson. 156 (2002) 79-96.

[69] P. E. Kristiansen, M. Carravetta, W. C. Lai, M. H. Levitt, A robust pulse sequence for the determination of small homonuclear dipolar couplings in magic-angle spinning NMR, Chem. Phys. Lett. 390 (2004) 1-7.

[70] P. E. Kristiansen, M. Carravetta, J. D. van Beek, W. C. Lai, M. H. Levitt, Theory and applications of supercycled symmetry-based recoupling sequences in solid-state nuclear magnetic resonance, J. Chem. Phys. 124 (2006) 234510.

[71] A. Brinkmann, A. P. M. Kentgens, Sensitivity enhancement and heteronuclear distance measurements in biological ^{17}O solid-state NMR, J. Phys. Chem. B, 110 (2006) 16089-16101.

[72] A. Brinkmann, A. P. M. Kentgens, Proton-selective ^{17}O-^{1}H distance measurements in fast magic-angle-spinning solid-state NMR spectroscopy for the determination of hydrogen bond lengths, J. Am. Chem. Soc. 128 (2006) 14758-14759.

[73] P. K. Madhu, X. Zhao, M. H. Levitt, High-resolution ^{1}H NMR in the solid state using symmetry-based pulse sequences, Chem. Phys. Lett. 346 (2001) 142-148.

[74] S. Paul. R. S. Thakur, P. K. Madhu, ^{1}H homonuclear dipolar decoupling at high magic-angle spinning frequencies with rotor-synchronised symmetry sequences, Chem. Phys. Lett. 456 (2008) 253-256.

[75] S. Paul, R. S. Thakur, M. H. Levitt, P. K. Madhu, ^{1}H homonuclear dipolar decoupling using rotor synchronized pulse sequences: Towards pure absorption phase spectra, J. Magn. Reson. 205 (2010) 269-275.

[76] S. Paul. D. Schneider, P. K. Madhu, ^{1}H Homonuclear dipolar decoupling using symmetry-based pulse sequences at ultra fast magic-angle spinning frequencies, J. Magn. Reson. 206 (2010) 241-245.

[77] H. Nagashima, J. Trébosc, O. Lafon, F. Pourpoint, P. Paluch, M. J. Potrzebowski, J.-P. Amoureux, Imaging the spatial distribution of radiofrequency field, sample and temperature in MAS NMR rotor, Solid State Nucl. Magn. Reson. 87 (2017) 137-142.

[78] Z. Tošner, A. Purea, J. O. Struppe, S. Wegner, F. Engelke, S. J. Glaser, B. Reif, Radiofrequency fields in MAS solid state NMR probes, J. Magn. Reson. 284 (2017) 20-32.

[79] Z. Tošner, R. Sarkar, J. Becker-Baldus, C. Glaubitz, S. Wegner, F. Engelke, S. J. Glaser, B. Reif, Overcoming volume selectivity of dipolar recoupling in biological solid-state NMR spectroscopy, Angew. Chem. Int. Ed. (2018) in press.

[80] H.-L. Jian, N. Tsumori, Q. Xu, A series of (6,6)-connected porous lanthanide-organic framework enantiomers with high thermostability and exposed metal sites: scalable syntheses, structures, and sorption properties, Inorg. Chem. 49 (2010) 10001-10006.

[81] J. Luo, H. Xu, Y. Liu, Y. Zhao, L. L. Daemen, C. Brown, T. V. Timofeeva, S. Ma, H.-C. Zhou, Hydrogen adsorption in a highly stable porous rare-earth metal-organic framework: sorption properties and neutron diffraction studies, J. Am. Chem. Soc. 130 (2008) 9626-9627.

[82] N. L. Rosi, J. Kim, M. Eddaoudi, B. Chen, M. O'Keefe, O. M. Yaghi, J. Am. Chem. Soc. 127 (2005) 1504-1518.

[83] J. R. Yates, C. J. Pickard, F. Mauri, Calculation of NMR chemical shifts for extended systems using ultrasoft pseudopotentials, Phys Rev. B 76 (2007) 024401.

[84] M. Profeta, F. Mauri, C. J. Pickard, Accurate First principles prediction of ^{17}O NMR parameters in SiO_2: assignment of the zeolite ferrierite spectrum, J. Am. Chem. Soc. 125 (2003) 541-548.

[85] C. Bonhomme, C. Gervais, F. Babonneau, C. Coelho, F. Pourpoint, T. Azaïs. S. E. Ashbrook, J. M. Griffin, J. R. Yates, F. Mauri, C. J. Pickard, First principles calculation of NMR parameters

using the gauge including projector augmented wave method: A chemist's point of view, Chem. Rev. 112 (2012) 5733-5779.

[86] P. D. Battle, B. Montez, E. Oldfield, The characterization of anion-vacancy ordering in the oxide ion conductor $(Bi_2O_3)_{1-x}(Y_2O_3)_x$ by ^{89}Y N.M.R. spectroscopy, J. Chem. Soc., Chem. Commun. (1988) 584-585.

[87] F. T. Edelmann, Scandium, yttrium, and the lanthanide and actinide elements, excluding their zero oxidation state complexes, Compr. Organomet. Chem. II 4 (1995) 11-212.

[88] J. R. Yates, C. J. Pickard, M. C. Payne, Relativistic nuclear magnetic resonance chemical shifts of heavy nuclei with pseudopotentials and the zeroth-order regular approximation, J. Chem. Phys. 118 (2003) 5746-5753.

[89] M. Bak, J. T. Rasmussen, N. C. Nielsen, SIMPSON: A general simulation program for solid-state NMR spectroscopy, J. Magn. Reson. 147 (2000) 296-330.

[90] Z. Tošner, R. Andersen, B. Stevensson, M. Edén, N. C. Nielsen, T. Vosegaard, Computer-intensive simulation of solid-state NMR experiments using SIMPSON, J. Magn. Reson. 246 (2014) 79-93.

[91] M. Bak, N. C. Nielsen, REPULSION, A novel approach to efficient powder averaging in solid-state NMR, J. Magn. Reson. 125 (1997) 132-139.

[92] P. Hohenberg, W. Kohn, Inhomogeneous electron gas, Phys. Rev. B 136 (1964) 864-871.

[93] W. Kohn, L. J. Sham, Self-consistent equations including exchange and correlation effects, Phys. Rev. 140 (1965) 1133-1138.

[94] J. P. Perdew, K. Burke, M. Ernzerhof, Generalized gradient approximation made simple, Phys. Rev. Lett. 77 (1996) 3865-3868.

[95] P. E. Blöchl, Projector augmented-wave method, Phys. Rev. B 50 (1994) 17953-17979

[96] G. Kresse, J. Furthmüller, Efficient iterative schemes for *ab initio* total-energy calculations using a plane-wave basis set, Phys. Rev. B 54 (1996) 11169-11186.

[97] G. Kresse, J. Furthmüller, Efficiency of ab-initio total energy calculations for metals and semiconductors using a plane-wave basis set, Comput. Mater. Sci. 6 (1996) 15-50.

[98] C. J. Pickard, F. Mauri, All-electron magnetic response with pseudopotentials: NMR chemical shifts, Phys. Rev. B 63 (2001) 245101.

[99] H. J. Monkhorst, J. D. Pack, Special points for Brillouin-zone integrations, 13 (1976) 5188-5192.